J. Fluid Mech. (1996), vol. 328, pp. 229–252

Wave pattern formation in a fluid annulus with a radially vibrating inner cylinder

By T. S. KRASNOPOLSKAYA† AND G. J. F. VAN HEIJST

Fluid Dynamics Laboratory, Department of Physics, Eindhoven University of Technology, PO Box 513, 5600 MB Eindhoven, The Netherlands

(Received 21 August 1995 and in revised form 22 July 1996)

The phenomenon of pattern formation of free-surface waves of a fluid confined in an annulus the inner wall of which vibrates radially, is investigated both theoretically and experimentally. Although the waves are excited by harmonic axisymmetric deformations of the inner shell, depending on the vibration frequency both axisymmetric and non-symmetric wave patterns may arise.

Experimental observations have revealed that waves are excited in two different resonance regimes. The first type corresponds to forced resonance, in which axisymmetric patterns are realized with eigenfrequencies equal to the frequency of excitation. The second kind is parametric resonance, in which case the waves are 'transverse', with their crests and troughs aligned perpendicular to the vibrating wall. These so-called cross-waves have frequencies equal to half of that of the wavemaker.

Both kinds of resonance were investigated theoretically using Lamé's method of superposition. It was shown experimentally that the pure forced resonant standing waves are not realized when the amplitude of excitation is beyond the threshold of parametric resonance for non-symmetric waves. The experimental observations agree very well with the theoretical results.

1. Introduction

It is well known that vibrating bodies (partially) immersed in a fluid may generate various types of wave patterns at the free surface of the fluid. An example is the formation of cross-waves, as first discussed by Faraday (1831). In his pioneering experiments, Faraday observed the occurrence of cross-waves at the surface of a vibrating plate immersed in a fluid. Cross-waves have crests perpendicular to the wavemaker (hence their name), and their frequency is half that of the wavemaker. As discussed in the review paper of Miles & Henderson (1990), cross-waves emerge from a symmetry-breaking instability of the directly forced wave motion.

Cross-waves have been the subject of many studies during the last 25 years or so (for a detailed survey, see Miles & Henderson 1990). It was Garrett (1970) who first showed how energy is transferred from the wavemaker to the cross-wave in a mathematical model including a mean motion of the free surface. He mentioned, however, that the primary (mean) motion of the free surface is not sufficient to supply the energy to the cross-waves. Therefore, the cross-waves must derive their energy in some way directly from the wavemaker.

† On leave from Institute of Mechanics, National Academy of Sciences of Ukraine, 252057 Kiev, Ukraine.

In the experimental work of Tatsuno, Inoue & Okabe (1969) the transition from longitudinal to cross-waves at a vertically vibrating half-submerged spherical body was studied for the first time. For the linear case this problem was described analytically by Hocking (1988) and for nonlinear case it was solved by Becker & Miles (1992). Becker & Henderson (see Appendix to Becker & Miles 1991) have repeated the original experiment of Tatsuno *et al.* (1969), although no recordings of the various wave patterns were given, probably because the main goal of that paper was the theoretical analysis of the radial cross-waves. Taneda (1991) performed similar experiments, and he presents a comprehensive set of photographs of the visualized motion induced by the oscillating sphere. Taneda kept the excitation frequency constant, but by increasing the amplitude of the sphere oscillation he observed the transformation of directly forced axisymmetric waves into parametrically excited non-symmetrical patterns. Similar observations were made by Taneda (1994) for the case of a half-submerged vertically oscillating horizontal cylinder of finite length.

In a theoretical study, Becker & Miles (1991) investigated the behaviour of cross-waves in an annular fluid region induced by radial vibrations of the inner cylinder. These authors made a modification to Havelock's (1929) solution of the wavemaker problem, and their solution contains all the information about the behaviour of axisymmetric modes and the influence of these modes on the stability of the resonant cross-wave. In Krasnopolskaya & Podchasov (1992*a*,*b*) the transition from longitudinal waves to cross-waves was studied in an annular fluid tank for a rotational wave deformation of the surface of the inner cylinder. The theoretical approach applied in those papers was based on the variational principle of Luke (1967). In the present study we will address the same wave-tank configuration, but we use a different method for solving the wavemaker problem, applying Lamé's (1852) superposition method. This method allows one to construct a simpler mathematical model, which shows how the cross-wave can be generated directly by the wavemaker motion without having to take into account the presence of any axisymmetric waves at the free surface. This simpler mathematical model of the excitation of the resonant cross-waves may be the easiest way to understand pattern formation on the fluid's free surface, the stability of the system and the influence of other modes with eigenfrequencies close to the resonant mode (the frequency spectrum is usually very dense), since these modes can be considered as also being under parametric resonance. In addition to this theoretical analysis we have carried out laboratory experiments in an annular wave tank with a radially vibrating inner cylinder. The resonant wave patterns resulting for different excitation frequencies were recorded photographically, and the transition from directly forced axisymmetric waves to parametrically excited non-axisymmetric patterns has been observed. Accurate measurements with a wave gauge have provided important information about the spectral characteristics of the two types of resonance.

The paper is organized as follows. In §2 we describe the laboratory configuration as well as some observed typical wave patterns and their spectral characteristics. The theoretical analysis of both the axisymmetric and the non-axisymmetric resonance modes is presented in §3. A comparison between the laboratory measurements and the theoretical results is described in §4.

2. Laboratory experiments

2.1. *Experimental arrangement*

The experiments were performed in a cylindrical tank with an inner diameter $2R_2 =$ 28.8 cm and a total depth of 20 cm. An inner cylinder with diameter $2r_1 = 9.0$ cm

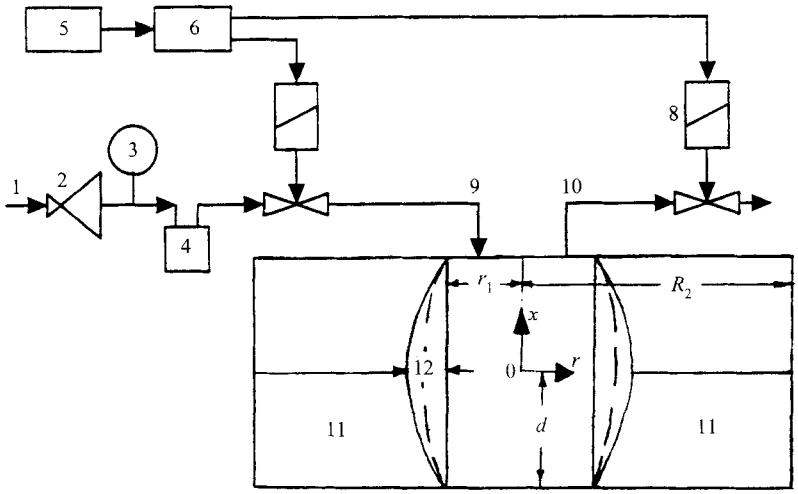

FIGURE 1. Schematic of the experimental set-up: 1, gas supply; 2, pressure regulator; 3, manometer; 4, pressure vessel; 5, frequency generator; 6, magnetic valve drive; 7 and 8, magnetic valves; 9, gas inlet; 10, gas outlet; 11, working fluid; 12, rubber membrane with vibrations χ around the mean position $a_0 \cos \eta x$ (dashed line).

was placed coaxially in the tank, and the annular region was filled with ordinary tap water up to a depth $d = 9.0$ cm. The hollow inner cylinder was perforated and tightly covered by an elastic rubber membrane (thickness 0.08 cm) that was fixed by two flanges at the top and bottom. The air pressure inside this cylinder could be changed periodically by a control system as schematically shown in figure 1. By alternatingly opening and closing the magnetic valves 7 and 8 (see figure 1), respectively, the air pressure inside the cylinder could be varied periodically from 1.1 bar to 1.3 bar (overpressure), at a prescribed frequency ω. As a result, the rubber cover performed radial vibrations at this frequency ω. In terms of the cylindrical coordinates r, θ, x (with r the radial coordinate measured from the common axis, and x the axial coordinate, with $x = 0$ at the unperturbed free surface) the shape of the vibrating rubber sheet is to a good approximation represented by

$$\chi(x,t) = (a_0 + a_1 \cos \omega t) \cos \eta x, \tag{2.1}$$

where $\eta = \pi/d_0$, with $d_0 = 2d$ the axial size of the rubber cover. Note that d_0 is twice the water depth d, so that the maximum vibration amplitude occurs at the free surface. The amplitude coefficients a_0 and a_1 could be varied by changing the pressure in the inner cylinder (see figure 1), but in all cases $a_0 \geqslant a_1$ and $a_0 + a_1$ was approximately equal to 1 cm. Experiments were carried out for excitation frequencies $f_e = \omega/2\pi$ in the range 3 Hz to 30 Hz. In the experiments a_1 decreased from 0.4 cm for 3 Hz to 0.02 cm for 30 Hz, so that $a_0, a_1 \ll r_1$.

The wave patterns on the free surface of the fluid were visualized by an ordinary light source that was mounted beside the tank, directed at some angle to the fluid surface, and the patterns were recorded from above by a camera that was mounted at some distance above the tank.

The instantaneous surface elevations were locally measured by a conductance-type wave gauge, originally designed by Fryer & Thomas (1975). Although in the set-up described by these authors the probe consisted of two parallel metal wires, in our experiments a single wire was lowered vertically into fluid, while a metal plate was placed horizontally at the tank bottom. The conductance between the probe wire and

the plate is proportional to the immersion depth of the wire and the conductivity of the fluid. The conductance, and thus the probe immersion depth, can be measured by applying a potential difference between the wire and the plate and measuring the resulting electric current. For a constant fluid conductivity this current was found to be linearly proportional to the probe immersion depth. In order to increase the conductance, salt was added to the fluid (60 mg per litre tap water).

In most experiments the probe was placed at a distance of approximately 2.5 cm from the outer cylinder, with an immersion depth of typically 1 cm. For details of the electronic circuitry, the reader is referred to Fryer & Thomas (1975). The wave gauge signal was sampled by a personal computer and recorded (together with the signal of the frequency generator in the pressure control system) for further analysis.

2.2. *Some observations*

At relatively low excitation frequencies ($3 \leqslant f_e \leqslant 21.82$ Hz) the free surface of the fluid shows concentric, circular wave patterns, corresponding to directly excited axisymmetric waves with nodes at concentric circles between the two cylinders. An example of this type of wave pattern is shown in figure 2 for the case $f_e = 11.13$ Hz: the photograph (figure 2*a*) shows concentric black and white rings, which correspond to surface depressions and elevations, respectively. Owing to uneven illumination the rings visible on the photograph are slightly irregular, and in some cases not even closed. Visual *in situ* observations, however, revealed a perfectly circularly symmetric wave pattern, with nine nodes in the radial direction. Note that the wave pattern at some distance from the inner cylinder is that of standing waves: half a period later the areas of surface elevation have become areas of surface depression, and *vice versa*. The nodal circles thus approximately coincide with circular boundaries between the black and white rings. In a narrow band close to the inner cylinder, however, the wave motion is not that of standing waves, owing to the radial displacements of the cylindrical wall. This type of wave motion is observed on photographs like the one in figure 2(*a*) in the form of two thin white rings (rather than a single, wider ring) next to the wavemaker. The signal in mV of the wave gauge (placed at a distance 2.5 cm from the outer cylinder) is shown in figure 2(*b*), together with the signal of the frequency generator that drives the pressure valves, and therewith the wavemaker. Visual inspection reveals that it has a basic frequency that corresponds to that of the wavemaker. In order to make a more accurate comparison, the fast Fourier transforms (FFTs) of both signals are shown in figure 2(*c*) as a function of the frequency f_T. In this graph (and in similar graphs that will be presented later) the dashed curve represents the gas pressure change in the wavemaker, while the solid curve represents the measured wave signal. Although the FFTs could be determined for frequencies up to 1500 Hz, only the interval 1–100 Hz is shown because it contains the most relevant information. The pressure signal has a pronounced peak at the excitation frequency f_e and also some peaks at distinct higher frequencies, indicating higher-frequency components of the signal. The FFTs of the free-surface waves have the largest peak at the excitation frequency f_e, and a smaller one at a frequency $2f_e$. Since the FFT is a power spectrum (indicating the power contained at each frequency), the ratio of the peak heights corresponds to the ratio of the squared wave amplitudes (i.e. the wave energy) at those frequencies. Apparently, the directly excited mode contains approximately 83 times more energy than the wave mode with frequency $2f_e$.

The excitation frequency was systematically increased, and up to the value of 21.82 Hz only circular wave patterns were observed, with the number of nodal circles increasing with increasing frequency. While the excitation frequency was

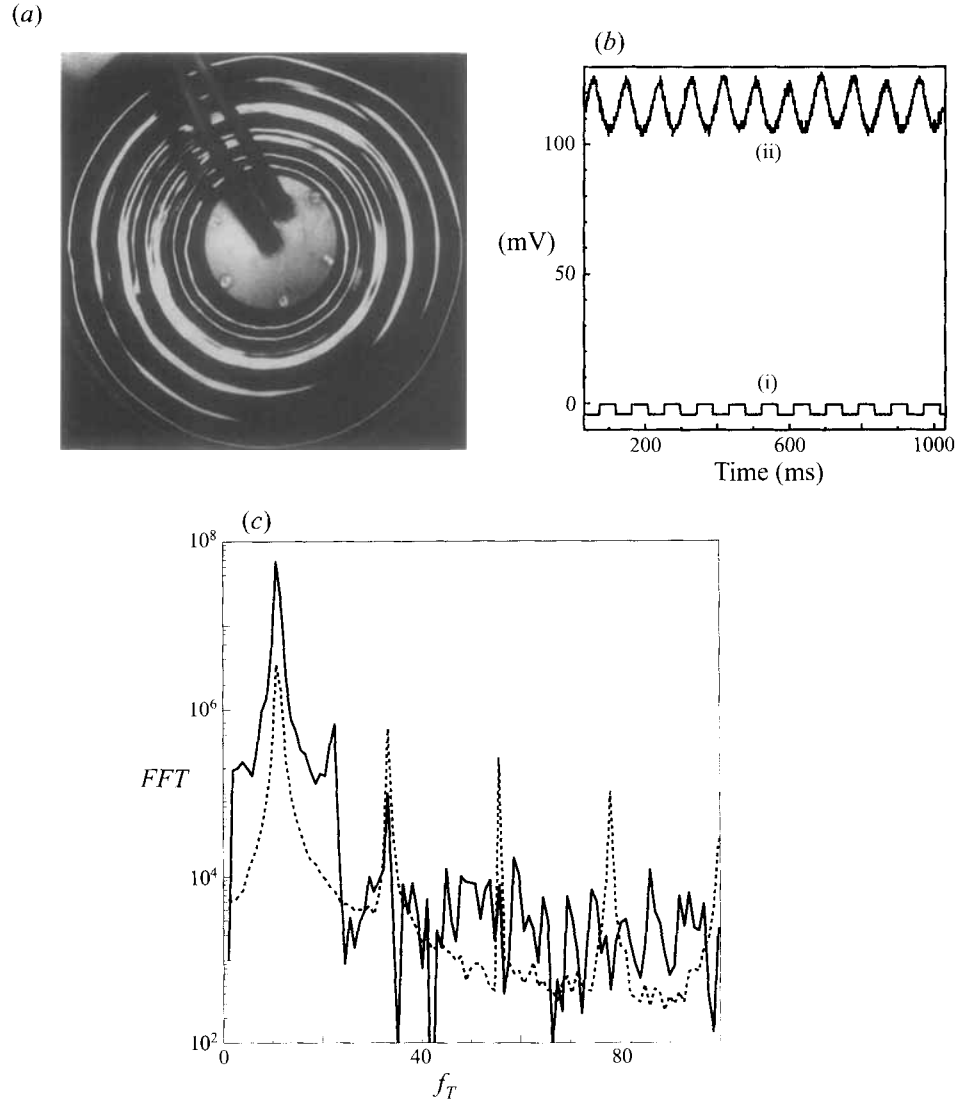

FIGURE 2. Wave activity at excitation frequency $f_e = 11.13$ Hz: (*a*) photograph showing the free-surface wave pattern; (*b*) pressure (i) and wave gauge (ii) signals; (*c*) FFTs of these signals.

systematically increased in the range $3 \leqslant f_e \leqslant 21.82$ Hz, the amplitude a_1 of the wavemaker oscillations decreased from 0.4 cm to 0.08 cm. The effective fluid-level rise in the annulus associated with the radial vibrations of the membrane (see (3.14)), was hence reduced from approximately 0.2 cm (with amplitude 0.1 cm) to approximately 0.04 cm. These fluid level oscillations were not observed to lead to any non-symmetrical pattern formation with frequency $0.5f_e$. On the contrary, only symmetrical patterns were observed whose FFTs had the largest peak at the excitation frequency f_e. We may thus conclude that the fluid level oscillations did not influence the pattern formation at the lower excitation frequency. This implies that the 'forced resonance mechanism' is apparently stronger than the mechanism of parametric variation of the gravitational acceleration of the fluid level at these low excitation frequencies.

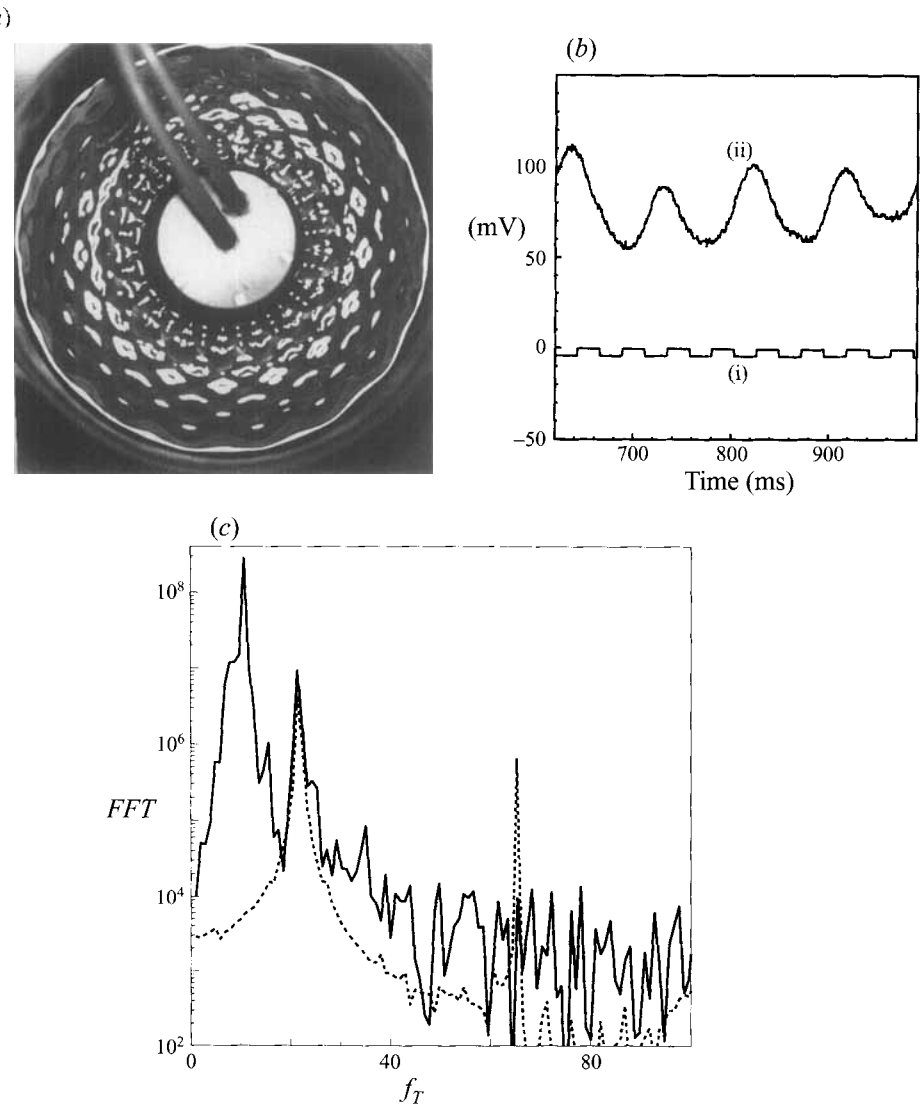

FIGURE 3. Wave activity at excitation frequency $f_e = 21.82$ Hz: (*a*) photograph showing the free-surface wave pattern; (*b*) pressure (i) and wave gauge (ii) signals; (*c*) FFTs of these signals.

While keeping the excitation amplitude of the wavemaker (i.e. the pressure variations) approximately constant at a value $a_1 = 0.08$ cm, the first non-axisymmetrical wave pattern was observed at excitation frequency $f_e = 21.82$ Hz†. A photograph of the recorded pattern is shown in figure 3(*a*), while the pressure and wave gauge signals and their FFTs are presented in figures 3(*b*) and 3(*c*), respectively. The photograph clearly reveals the azimuthal structure of the wave pattern, with white patches (surface elevations) arranged on circles of different radii. By counting the number of these patches on a certain radius, it is found that the azimuthal wavenumber is $n = 17$ (independent of the radius). The radial wavenumber can be determined in the

† It should be noted that in experiments with larger excitation amplitudes the transition to non-axisymmetric patterns was observed to occur at somewhat lower frequencies. For example, with amplitude $a_1 = 0.1$ cm, the transition occurred at $f_e = 19.96$ Hz.

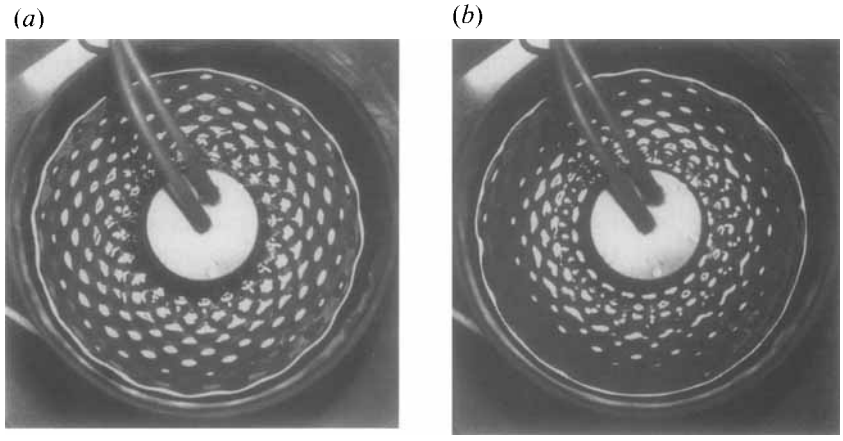

FIGURE 4. Photographs of the free-surface waves at excitation frequency $f_e = 26.00$ Hz: (*a*), (*b*) top views at different times

same way (although in a number of cases this is difficult to do from the photographs; direct visual observations may be helpful then), and from figure 3(*a*) one finds $m = 8$. Figure 3(*b*) shows that the basic frequency of the wave gauge signal is approximately equal to half the excitation frequency. This is observed even better in the FFTs of both signals, see figure 3(*c*): although the power spectrum of the surface waves shows a well-defined peak at the excitation frequency f_e, a much higher peak occurs at a frequency close to $0.5f_e$. The ratio of the peak values is about 28, which implies that the energy contained in the waves with frequency $\approx 0.5f_e$ is approximately 28 times larger than the energy of the waves with frequency f_e. In other words, the waves excited at frequency $\approx 0.5f_e$ contain about 96.5% of the energy present in these two types of waves, whereas those with frequency f_e contain only 3.5%. This difference was even larger in an experiment with a larger vibration amplitude, in which the non-axisymmetrical pattern occurred at $f_e = 19.96$ Hz. The ratio of the energies contained in both types of waves was found to be close to 150, implying that in this case the directly excited waves (at frequency f_e) contain only 0.6% of the energy, while those with frequency $\approx 0.5f_e$ carry 99.4%. For this case the fluid level oscillations with frequency f_e were negligibly small, having an amplitude at least 12 times smaller than that of the non-symmetrical pattern, which rules out their role in the excitation of the non-symmetric waves. As will be discussed in detail in §3.2, the direct wavemaker excitation is the principal generation mechanism for the non-symmetric pattern.

Both the azimuthal and the radial wavenumber of the wave pattern increases with increasing excitation frequency. Figures 4(*a*) and 4(*b*) show two photographs of the free-surface pattern excited at $f_e = 26.00$ Hz, taken at different moments. Analysis of the photographs yields $n = 20$, $m = 10$. The power spectra of the pressure and wave gauge signals show the same features as in the non-axisymmetrical case with $f_e = 21.82$ Hz (see figure 3*c*); again most (97%) of the energy is contained in the wave excited at half the wavemaker's frequency, rather than in the directly excited wave with the frequency f_e.

The maximum frequency that could be reached with the laboratory configuration was $f_e = 30.10$ Hz. In that case one observes a pattern essentially similar to the other non-axisymmetric cases, now with $n = 25$ and $m = 11$. Again, the wave with frequency $0.5f_e$ contains most of the energy.

From these experimental observations, carried out at different excitation frequencies, we can conclude that, although the excitation is purely axisymmetric, two kinds of resonance regimes exist. The first type is forced resonance, in which the free-surface waves are circular, with a frequency equal to the excitation frequency f_e. The second type of resonance is the so-called parametric resonance, in which the excited waves are transverse, i.e. with their crests and troughs aligned perpendicular to the vibrating wall. The latter type of resonance appears through symmetry-breaking (note that the excitation is purely axisymmetric, i.e. without any azimuthal modes), and occurs with a frequency of approximately $0.5f_e$. Moreover, in the cases considered, the energy carried by the parametrically excited cross-waves is at least 20 times larger than that contained by the directly forced waves. From this fact one may conclude that the cross-waves derive their energy directly from the wavemaker rather than from the axisymmetric (or other) waves with frequency f_e, since these only contain a very small portion of the wave energy.

3. Theoretical analysis

Now we will theoretically consider the specific features of both types of resonance. It is useful to relate the fluid motion to the cylindrical coordinate system (r, θ, x) introduced in the previous section. The fluid has an average depth d; the average position of the free surface is taken as $x = 0$, so that the solid tank bottom is at $x = -d$. The fluid is confined between a solid outer cylinder at $r = R_2$ and a deformable inner cylinder at average radius $R_1 = r_1 + a_0(d)^{-1} \int_{-d}^{0} \cos \eta x \mathrm{d}x = r_1 + 2a_0/\pi$. This inner cylinder acts as the wavemaker and vibrates harmonically in such a way that the position of the wall of the inner cylinder is $r = r_1 + \chi(x,t) = R_1 + \chi_1(x,t)$, with χ given by (2.1) and $\chi_1 = \chi - 2a_0/\pi$.

Assuming that the fluid is inviscid and incompressible, and that the induced motion is irrotational, the velocity field can be written as $\boldsymbol{v} = \nabla\phi$, with $\phi(r, \theta, x, t)$ the velocity potential. The governing equation is

$$\nabla^2\phi = 0 \qquad \text{on} \qquad (R_1 + \chi_1 \leqslant r \leqslant R_2, 0 \leqslant \theta \leqslant 2\pi, -d \leqslant x \leqslant \zeta) \tag{3.1}$$

where $\zeta(r, \theta, t)$ is free-surface displacement.

The dynamic and kinematic free-surface boundary conditions are

$$\phi_t + \tfrac{1}{2}(\nabla\phi)^2 + g\zeta = \frac{T}{\rho}[\nabla^2\zeta - \tfrac{1}{2}\nabla\zeta \cdot ((\nabla\zeta)^2\nabla\zeta)] + F(t) \qquad \text{at} \qquad x = \zeta(r, \theta, t), \tag{3.2}$$

$$\phi_x = \nabla\phi \cdot \nabla\zeta + \zeta_t \qquad \text{at} \qquad x = \zeta(r, \theta, t), \tag{3.3}$$

with g the gravitational acceleration, T the air–fluid surface tension and ρ the fluid density, $F(t)$ is an arbitrary function of time (Lamb 1932). Here and later the subscripts x, r, θ, t signify partial differentiation.

The normal velocity vanishes at the solid flow boundaries:

$$\phi_r = 0 \qquad \text{at} \qquad r = R_2, \tag{3.4}$$

$$\phi_x = 0 \qquad \text{at} \qquad x = -d, \tag{3.5}$$

while the kinematic condition at the vibrating inner cylinder is

$$\phi_r = \chi_t + \nabla\phi \cdot \nabla\chi \qquad \text{at} \qquad r = R_1 + \chi_1(x,t). \tag{3.6}$$

Effects of the meniscus and capillarity at the contact line of the fluid's free surface and the annular container walls were not incorporated in the formulation of the problem. We assume that $\zeta_r = 0$ at $r = R_1$ and $r = R_2$.

From the experimental observations we may conclude that the pattern formation has a resonance character, every pattern having its 'own' frequency. Assuming that patterns can be described in terms of normal modes with characteristic eigenfrequencies, we expand the potential ϕ and the free-surface displacement ζ in a complete set of eigenfunctions, which are determined by linear theory. The amplitudes of these eigenfunctions are governed by the nonlinear problem (3.2)–(3.3).

The solution of the linear general non-axisymmetric boundary problem

$$\nabla^2\phi = 0 \qquad \text{on} \qquad (R_1 \leqslant r \leqslant R_2, 0 \leqslant \theta \leqslant 2\pi, -d \leqslant x \leqslant 0), \tag{3.7}$$

$$\phi_x = \zeta_t \qquad \text{at} \qquad x = 0, \tag{3.8a}$$

$$\phi_x = 0 \qquad \text{at} \qquad x = -d, \tag{3.8b}$$

$$\phi_r = 0 \qquad \text{at} \qquad r = R_2, \tag{3.8c}$$

$$\phi_r = \chi_t \qquad \text{at} \qquad r = R_1, \tag{3.8d}$$

$$\phi_\theta\,|_{\theta=0} = \phi_\theta\,|_{\theta=2\pi}, \tag{3.8e}$$

under arbitrary excitation of the inner cylindrical shell $w(\theta, x, t)$ can be found in several ways. One of them traces back to Stokes's paper dated 1847 (see Bromwich 1959, Art. 128), also known as Grinberg's method (Lebedev, Skal'skaya & Uflyand 1966, Ch. V). Here the potential ϕ is presented as Fourier series of the complete system of eigenfunctions in the radial and azimuthal coordinates with the coefficients as functions of the coordinate x. The inhomogeneous boundary condition at $r = R_1$ is transformed into the right-hand side of equation (3.7) using the ordinary procedure of the Fourier series representation for the derivatives on r. The solutions of the sequence of inhomogeneous linear differential equations in x for the expansion coefficients with inhomogeneous boundary conditions in x can be easily found by analytical techniques. This approach yields, however, rather cumbersome expressions, in which the input of the wavemaker motion $w(\theta, x, t)$ is not seen in a clear way.

In order to obtain a more lucid picture of the transmission from the wavemaker motion to the free-surface motion it is more convenient to use another analytical method, namely, the method of superposition. The authors are of the opinion that the application of this method is without doubt preferable for the problem in question. It provides a clear physical picture of the mechanism of energy transfer from the wavemaker to the mean level variation and every eigenmode of free-surface oscillations. The idea of the superposition method was first proposed by Lamé (1852) in his classical lectures on the theory of elasticity. A similar method was applied by Hocking & Mahdmina (1991) to study moving capillary–gravity waves produced by a wavemaker.

According to this superposition method, the potential ϕ can be written as the sum of three harmonic functions:

$$\phi = \phi_0 + \phi_1 + \phi_2. \tag{3.9}$$

The potential ϕ_0 is governed by the following axisymmetric boundary problem:

$$\nabla^2\phi_0 = 0 \qquad \text{on} \qquad (R_1 \leqslant r \leqslant R_2, 0 \leqslant \theta \leqslant 2\pi, -d \leqslant x \leqslant 0), \tag{3.10}$$

$$(\phi_0)_x = (\zeta_0)_t \quad \text{at} \quad x = 0, \tag{3.11a}$$

$$(\phi_0)_x = 0 \quad \text{at} \quad x = -d, \tag{3.11b}$$

$$(\phi_0)_r = 0 \quad \text{at} \quad r = R_2, \tag{3.11c}$$

$$(\phi_0)_r = (w_0)_t \quad \text{at} \quad r = R_1, \tag{3.11d}$$

$$(\phi_0)_\theta \,|_{\theta=0} = (\phi_0)_\theta \,|_{\theta=2\pi}, \tag{3.11e}$$

where

$$\zeta_0(t) = \frac{1}{\pi(R_2^2 - R_1^2)} \int_0^{2\pi} \int_{R_1}^{R_2} \zeta(r, \theta, t) r \mathrm{d}r \mathrm{d}\theta, \tag{3.12a}$$

$$w_0(t) = \frac{1}{2\pi R_1 d} \int_0^{2\pi} \int_{-d}^{0} w(\theta, x, t) R_1 \mathrm{d}x \mathrm{d}\theta \tag{3.12b}$$

represent the mean level elevation of the fluid free surface and mean displacement of the cylindrical wavemaker, respectively. These mean values are connected by the relationship

$$(\zeta_0)_t \pi(R_2^2 - R_1^2) - 2\pi d R_1 (w_0)_t = 0 \tag{3.13}$$

expressing mass conservation for the incompressible fluid. Thus, for the particular case of the wavemaker excitation (2.1) it is easy to derive from this relationship the mean level oscillation:

$$\zeta_{00}(t) = \frac{4R_1 d}{\pi(R_2^2 - R_1^2)} (a_1 \cos \omega t). \tag{3.14}$$

The potential ϕ_1 is governed by the following linear problem:

$$\nabla^2 \phi_1 = 0 \quad \text{on} \quad (R_1 \leqslant r \leqslant R_2, 0 \leqslant \theta \leqslant 2\pi, -d \leqslant x \leqslant 0), \tag{3.15}$$

$$(\phi_1)_x = (\zeta - \zeta_0)_t \quad \text{at} \quad x = 0, \tag{3.16a}$$

$$(\phi_1)_x = 0 \quad \text{at} \quad x = -d, \tag{3.16b}$$

$$(\phi_1)_r = 0 \quad \text{at} \quad r = R_2, \tag{3.16c}$$

$$(\phi_1)_r = 0 \quad \text{at} \quad r = R_1, \tag{3.16d}$$

$$(\phi_1)_\theta \,|_{\theta=0} = (\phi_1)_\theta \,|_{\theta=2\pi}, \tag{3.16e}$$

where the conditions in the radial direction are homogeneous and in the azimuthal direction periodic. So ϕ_1 will be expressed as a sum of complete systems of eigenfunctions in the radial and azimuthal coordinates.

While the potential ϕ_2 is governed by

$$\nabla^2 \phi_2 = 0 \quad \text{on} \quad (R_1 \leqslant r \leqslant R_2, 0 \leqslant \theta \leqslant 2\pi, -d \leqslant x \leqslant 0), \tag{3.17}$$

$$(\phi_2)_x = 0 \quad \text{at} \quad x = 0, \tag{3.18a}$$

$$(\phi_2)_x = 0 \quad \text{at} \quad x = -d, \tag{3.18b}$$

$$(\phi_2)_r = 0 \quad \text{at} \quad r = R_2, \tag{3.18c}$$

$$(\phi_2)_r = (w - w_0)_t \quad \text{at} \quad r = R_1, \tag{3.18d}$$

$$(\phi_2)_\theta \,|_{\theta=0} = (\phi_2)_\theta \,|_{\theta=2\pi}, \tag{3.18e}$$

it can be represented as a sum of eigenfunctions in the vertical (homogeneous

The boundary condition (3.16*a*) provides a relation between the amplitudes of the series (3.20) and (3.25) in the form

$$\phi_{ij}^{c,s}(t) = \dot{\zeta}_{ij}^{c,s}(t)(k_{ij}\tanh k_{ij}d)^{-1}. \tag{3.26}$$

The velocity potential $\phi_2(r,\theta,x,t)$ can be formulated in terms of an ordinary Fourier series in $\cos\alpha_l x$ with $\alpha_l = l\pi/d$ and in $(\cos i\theta, \sin i\theta)$, so that the general solution reads

$$\phi_2 = \sum_{i=0}^{\infty}\sum_{l=1}^{\infty} \Phi_{il}^{c,s}(t)\cos\alpha_l x\hat{\chi}_{il}(\alpha_l r)(\cos i\theta, \sin i\theta), \tag{3.27}$$

with

$$\hat{\chi}_{il}(\alpha_l r) = I_i(\alpha_l r) - \frac{I_i'(\alpha_j R_2)}{K_i'(\alpha_j R_2)}K_i(\alpha_l r), \tag{3.28}$$

where I_i and K_i are the ith-order modified Bessel functions of the first and second kind, respectively.

Using the boundary condition (3.18*d*) we can explicitly define the amplitudes $\Phi_{il}^{c,s}(t)$ as

$$\Phi_{il}^{c,s}(t) = \dot{w}_{il}^{c,s}(t)$$

$$= \frac{2-\delta_{i0}}{d\pi\alpha_l\hat{\chi}_{il}'(\alpha_l R_1)}\int_0^{2\pi}\int_{-d}^{0}[\dot{w}(\theta,x,t) - \dot{w}_0(t)]\cos\alpha_l x(\cos i\theta, \sin i\theta)R_1\,\mathrm{d}x\mathrm{d}\theta, \tag{3.29}$$

where δ_{i0} is the Dirac function and $\hat{\chi}_{0l}'(z) = \mathrm{d}\hat{\chi}_{0l}(z)/\mathrm{d}z$.

To define the unknown functions $\zeta_{ij}^{c,s}(t)$, representing the amplitudes of directly excited free-surface waves, we have to apply the linearized dynamic free-surface boundary condition (3.2):

$$\phi_t + g\zeta - \frac{T}{\rho}\nabla^2\zeta = F(t) \qquad \text{at} \qquad x = 0, \tag{3.30}$$

where ϕ represents the total velocity potential according to (3.9). Substitution of (3.9) into (3.30) leads to a functional equation in r in the interval (R_1, R_2). Representing the radial functions $r^2/2 - R_2^2\ln r$ and $\hat{\chi}_{il}(\alpha_l r)$ in the form of the expansions

$$\frac{r^2}{2} - R_2^2\ln r = a_{00} + \sum_{j=1}^{\infty} a_{0j}\frac{\chi_{0j}(k_{0j}r)}{N_{0j}}, \tag{3.31}$$

$$\hat{\chi}_{il}(\alpha_l r) = b_{il0} + \sum_{j=1}^{\infty} b_{ilj}\frac{\chi_{ij}(k_{ij}r)}{N_{ij}}, \tag{3.32}$$

where the coefficients a_{00}, a_{0j}, b_{i0l} and b_{ilj} can be found by straightforward integration, we can write down the infinite sequence of ordinary differential equations for the functions $\zeta_{ij}^{c,s}(t)$:

$$\ddot{\zeta}_{0j}(t) + \omega_{0j}^2\zeta_{0j}(t) = \ddot{w}_0(t)\frac{a_{0j}\beta_{0j}R_1}{(R_2^2 - R_1^2)} - \sum_{l=1}^{\infty}\ddot{w}_{0l}^{c}(t)b_{0lj}\beta_{0j}, \tag{3.33a}$$

$$\ddot{\zeta}_{ij}^{c,s}(t) + \omega_{ij}^2\zeta_{ij}(t) = -\sum_{l=1}^{\infty}\ddot{w}_{il}^{c,s}(t)b_{ilj}\beta_{ij}, \tag{3.33b}$$

where $\beta_{ij} = k_{ij} \tanh k_{ij} d$ and

$$\omega_{ij} = \left[\left(gk_{ij} + \frac{T}{\rho} k_{ij}^3\right) \tanh k_{ij} d\right]^{1/2} \quad \text{for} \quad i = 0, 1, 2, \ldots \quad \text{and} \quad j = 1, 2, 3, \ldots . \tag{3.34}$$

The linear equations (3.33*a,b*) represent typical equations of the forced oscillations with eigenfrequencies ω_{ij}. Solving these linear differential equations with specified initial conditions under prescribed time dependence of the functions $w_0(t)$ and $w_{il}^{c,s}(t)$, we can easily obtain the amplitudes $\zeta_{ij}(t)$ of the fluid free-surface waves in an explicit manner.

In the subsequent sections the nonlinear problems for resonant eigenmodes will be solved in the same way. First, to find the amplitudes of the potential ϕ_2 the nonlinear boundary condition (3.6) is applied with the expansion precedure in the series with $\cos \alpha_l x$ and $(\cos i\theta, \sin i\theta)$ functions. The second step is to determine the relations between the amplitudes of potential ϕ_1, the functions $\phi_{ij}(t)$ and the amplitudes $\zeta_{ij}(t)$ of the fluid free-surface waves according to the nonlinear boundary condition (3.3). And finally, the dynamic condition (3.2) is taken into consideration for the closure step, namely, to obtain nonlinear differential equations for resonant amplitudes under the prescribed excitation $\chi(x, t)$ given by (2.1).

3.1. *Symmetric patterns*

First we examine the appearance of axisymmetric free-surface wave patterns under forced resonance, when

$$\omega \approx \omega_{0m}, \tag{3.35}$$

with ω_{0m} the eigenfrequency for the axisymmetric mode, given by (3.34) for $i = 0$.

We assume that the wave pattern at the free surface can be described by the eigenmode ψ_{0m}, corresponding to the eigenfrequency ω_{0m}, as

$$\zeta(r, \theta, t) \approx \frac{\zeta_{0m}(t)}{N_{0m}} \psi_{0m}(r) + \zeta_{00}. \tag{3.36}$$

In order to find the solution of the nonlinear problem for the amplitude of this eigenmode we introduce the small parameter

$$\epsilon = \frac{a_1 \omega_{0m}^2}{g}, \tag{3.37}$$

where a_1 is the amplitude of the wavemaker vibrations, which we assume to be small (we also take $a_0 \equiv \epsilon \beta_0$). Following Miles (1984*a,b,c*), we express the amplitude of this mode as

$$\zeta_{0m}(t) = \epsilon^{1/3} \lambda [p(\tau) \cos \omega t + q(\tau) \sin \omega t] + \epsilon^{2/3} \lambda [A_0(\tau) \cos 2\omega t + B_0(\tau) \sin 2\omega t + C_0(\tau)], \tag{3.38}$$

where $\lambda = k_{0m}^{-1} \tanh(k_{0m} d)$ and

$$\tau = \epsilon^{2/3} \omega t \tag{3.39}$$

is the dimensionless 'slow' time. If $\zeta(r, \theta, t)$ has the form (3.36), then ϕ_1 is approximated by

$$\phi_1 \approx \phi_{0m}(t) \psi_{0m}(r) \frac{\cosh k_{0m}(x + d)}{N_{0m} \cosh k_{0m} d} \tag{3.40}$$

because of the same expansion of the eigenfunction $\psi_{ij}^{c,s}(r, \theta)$, see (3.20) and (3.25).

To determine the amplitude $\phi_{0m}(t)$ we take into account the effect of the potentials ϕ_0 and ϕ_2 under the constraint of the nonlinear boundary conditions (3.3) and (3.6). The solution that satisfies the nonlinear condition (3.6), with the inner-wall vibration $\chi(x,t)$ given by (2.1), is

$$\phi_2 = -\frac{2\epsilon g}{\omega}\sin\omega t \sum_{l=1}^{\infty} \frac{\cos\alpha_l x \hat{\chi}_{0l}(\alpha_l r)}{\alpha_l d\hat{\chi}'_{0l}(\alpha_l R_1)} \int_{-d}^{0} \cos\eta x \cos\alpha_l x \mathrm{d}x + O(\epsilon^{4/3})$$

$$= -\frac{2\epsilon g}{\omega}\sin\omega t \sum_{l=1}^{\infty} \frac{(-1)^l \eta \cos\alpha_l x \hat{\chi}_{0l}(\alpha_l r)}{(\alpha_l^2 - \eta^2)\alpha_l d\hat{\chi}'_{0l}(\alpha_l R_1)} + O(\epsilon^{4/3}) \tag{3.41}$$

and

$$\left.\begin{aligned} \phi_0 &= \frac{2\epsilon g R_1}{\pi\omega(R_2^2 - R_1^2)}\sin\omega t\left(\frac{r^2}{2} - R_2^2 \ln r\right) + \dot{\zeta}_{00}\frac{(d+x)^2}{2d}, \\ \zeta_{00} &= \frac{4\epsilon d g R_1}{\pi\omega^2(R_2^2 - R_1^2)}\cos\omega t \end{aligned}\right\} \tag{3.42}$$

Taylor expansion of the nonlinear boundary conditions (3.3) and (3.2) about $x = 0$ leads to the following third-order reduced boundary conditions:

$$(\phi_1)_x + (\phi_0)_x + \zeta(\phi_1)_{xx} + \zeta^2(\phi_1)_{xxx} = \zeta_t + (\phi_1)_r\zeta_r + \frac{1}{r^2}(\phi_1)_\theta\zeta_\theta + (\phi_1)_{rx}\zeta\zeta_r$$

$$+ \frac{1}{r^2}(\phi_1)_{\theta x}\zeta\zeta_\theta \qquad \text{at} \qquad x = 0 \tag{3.43}$$

and

$$(\phi_1)_t + \zeta(\phi_1)_{tx} + (\phi_0)_t + (\phi_2)_t + \zeta^2(\phi_1)_{txx} + g\zeta + \frac{T}{\rho}\nabla^2\zeta + \tfrac{1}{2}[(\phi_1)_x^2 + (\phi_1)_r^2 + \frac{1}{r^2}(\phi_1)_\theta^2]$$

$$+ (\phi_1)_x\zeta(\phi_1)_{xx} + (\phi_1)_r\zeta(\phi_1)_{rx} + \frac{1}{r^2}(\phi_1)_\theta\zeta(\phi_1)_{\theta x} = F(t) \qquad \text{at} \qquad x = 0. \tag{3.44}$$

In this derivation we took account of the condition (3.18*a*) and of the order of ϕ_2, see (3.41).

Application of the nonlinear boundary condition (3.43) (after multiplication by $\psi_{0m}(r)r/N_{0m}$ and integration over the distance between the two cylinders) yields the following result for the amplitude of ϕ_1:

$$\phi_{0m}(t) = \gamma_0[1 - \gamma_1\zeta_{0m} + \gamma_2\zeta_{0m}^2]\dot{\zeta}_{0m}(t). \tag{3.45}$$

Here $\dot{\zeta}_{0m}(t)$ is the time derivative of $\zeta_{0m}(t)$; furthermore,

$$\gamma_0 = [k_{0m}\tanh(k_{0m}d)]^{-1}. \tag{3.46}$$

The other constant coefficients are evaluated in the Appendix.

By substitution of the expression (3.45) into (3.44), multiplication by $\psi_{0m}(r)r/N_{0m}$, integration over the distance between the two cylinders and averaging over the fast time ωt, one finally obtains the evolution equations for the amplitudes p and q:

$$\frac{\mathrm{d}p}{\mathrm{d}\tau} = -[\beta + \tfrac{1}{2}A(p^2 + q^2)]q, \tag{3.47a}$$

$$\frac{\mathrm{d}q}{\mathrm{d}\tau} = [\beta + \tfrac{1}{2}A(p^2 + q^2)]p, + \gamma \tag{3.47b}$$

and the amplitudes of the secondary harmonics

$$A_0 = \tfrac{1}{6}\lambda\gamma_3(p^2 - q^2); \qquad B_0 = \tfrac{1}{3}\lambda\gamma_3 pq; \qquad C_0 = \tfrac{1}{2}\lambda\gamma_4(p^2 + q^2), \tag{3.48}$$

with A, γ_3, γ_4 constant coefficients (see the Appendix), and

$$\left.\begin{aligned} \beta &= \frac{\omega^2 - \omega_{0m}^2}{\epsilon^{2/3}\omega^2} \\ \gamma &= \frac{4gk_{0m}^2}{\omega}\sum_{l=1}^{\infty}\frac{(-1)^l\eta b_{0lm}}{(\alpha_l^2 - \eta^2)\alpha_l\omega_{om}\hat{\chi}_{0l}'(\alpha_l R_1)d} - \frac{4gk_{0m}^2 R_1 a_{0m}}{\omega^2\pi(R_2^2 - R_1^2)}. \end{aligned}\right\} \tag{3.49}$$

Weak, linear damping may be incorporated at this stage by replacing $\mathrm{d}/\mathrm{d}\tau$ by $(\mathrm{d}/\mathrm{d}\tau + \alpha)$ in (3.47), where

$$\alpha = \frac{\delta_{0m}}{\epsilon^{2/3}} \tag{3.50}$$

and δ_{0m} is the ratio of actual to critical damping for free oscillations of the resonant mode (and $2\pi\delta_{0m}$ is the logarithmic decrement) (see Miles 1967). Therefore, we have

$$\frac{\mathrm{d}p}{\mathrm{d}\tau} = -\alpha p - [\beta + \frac{1}{2}A(p^2 + q^2)]q, \tag{3.51a}$$

$$\frac{\mathrm{d}q}{\mathrm{d}\tau} = -\alpha q + [\beta + \frac{1}{2}A(p^2 + q^2)]p + \gamma. \tag{3.51b}$$

Because of the presence of the term γ, which depends on the function of excitation (2.1) (and therefore on ϕ_0 and ϕ_2, see (3.41)–(3.42)), in the evolution equation (3.51b) and due to the nonlinear coupling of the equations, the axisymmetric resonance mode of the free fluid surface will have non-zero amplitudes p and q. The typical fixed-points solution which corresponds to harmonic motions ($\mathrm{d}p/\mathrm{d}\tau = 0; \mathrm{d}q/\mathrm{d}\tau = 0$) is given by

$$p^2 + q^2 = \frac{\gamma^2}{\alpha^2 + [\beta + A(p^2 + q^2)/2]^2}. \tag{3.52}$$

Thus, the amplitude of the resonant mode $\zeta_{0m}(t)$, see (3.38), has the order $O(\epsilon^{1/3})$ because of the realization of the resonance condition (3.35) (or, more precisely, the relation $\omega - \omega_{0m} = \epsilon^{2/3}\omega\beta/2$) with two non-zero components p and q. Other modes will have amplitudes of $O(\epsilon)$, as non-resonant modes are proportional to the amplitude of excitation.

So we have shown that axisymmetrical excitation (2.1) creates an axisymmetrical pattern which corresponds to one resonant symmetrical mode (under resonance condition $\omega = \omega_{0m} + \epsilon^{2/3}\omega\beta/2$).

3.2. *Non-symmetric patterns: resonance mode model*

Next we will consider the wave pattern that is realized during parametric resonance, when the excitation frequency ω, see (2.1), is twice as large as one of the eigenfrequencies, i.e.

$$\omega \approx 2\omega_{nm}. \tag{3.53}$$

In this case the excitation (2.1) selects vibrations with respect to the normal eigenmodes $\psi_{nm}^{c,s}$ ($n \neq 0$). So we consider a mathematical model in which the free-surface displacement can be approximated only by the resonance mode and the mean level displacement

$$\zeta \approx \frac{1}{N_{nm}}\zeta_{nm}(t)\psi_{nm}(r, \theta) + \zeta_{00}. \tag{3.54}$$

Here $\psi_{nm}(r,\theta) = \psi(r,\theta)$ can either be $\psi^c_{nm}(r,\theta)$ or $\psi^s_{nm}(r,\theta)$, since the angular momentum of the considered excitation is zero; arbitrarily, we take $\psi_{nm}(r,\theta) = \chi_{nm}(k_{nm}r)\cos n\theta$.

We seek the functions ζ_{nm} in the following form (see also Miles 1984*a*):

$$\zeta_{nm} = \epsilon_1^{1/2}\lambda_1[p_1(\tau_1)\cos(\tfrac{1}{2}\omega t) + q_1(\tau_1)\sin(\tfrac{1}{2}\omega t)] \tag{3.55}$$

where $\lambda_1 = k_{nm}^{-1}\tanh(k_{nm}d)$ is the reference length, $\epsilon_1 = a_1\omega_{nm}^2/g$ is a new small positive parameter, and

$$\tau_1 = \tfrac{1}{4}\epsilon_1\omega t \tag{3.56}$$

is a dimensionless slow time; the variables $p_1(\tau_1), q_1(\tau_1)$ are slowly varying dimensionless amplitudes of the dominant mode.

The most important term among the non-resonant modes (Garrett 1970; Becker & Miles 1991) is the primary (mean) motion $\zeta_{00}(t)$ (3.14). For the tank geometry as used in the experiments (when $R_2^2 - R_1^2 > R_1 d$)

$$\zeta_{00}(t) = 0.27a_1\cos\omega t + O(\epsilon_1^{3/2}). \tag{3.57}$$

The smallest value of ϵ_1 corresponds to the excitation frequency for the first non-symmetrical pattern. For $f_e = 19.96$ Hz, $\epsilon_1 = 0.4$ (when a_1=0.1 cm), so $\zeta_{00}(t)$ has $O(\epsilon_1^{3/2})$. For the last non-symmetrical pattern at $f_e = 30.1$ Hz, $\zeta_{00}(t)$ has $O(\epsilon_1^2)$. Thus, $\zeta_{00}(t)$ is negligibly small; however for the case of a basin when $R_2^2 - R_1^2 < R_1 d$, the mean motion $\zeta_{00}(t)$ may be important. The oscillations ζ_{00} will not be incorporated in the nonlinear terms of the boundary conditions when keeping the terms to the third order, namely to $O(\epsilon_1^{3/2})$, because in the geometry considered the solutions of the linear problem for ζ_{00} (3.57) are evaluated as corresponding to $O(\epsilon_1^{3/2})$. Nevertheless, the influence of the potential ϕ_0, expressed by (3.42) with $\epsilon_1 = \epsilon/4$, will be taken into account in the nonlinear terms of the boundary conditions.

For free-surface vibrations of the form (3.54), it can be assumed that the velocity potential ϕ_1 contains the term

$$\phi_1 \approx \phi_{nm}(t)\psi_{nm}(r,\theta)\frac{\cosh k_{nm}(x+d)}{N_{nm}\cosh k_{nm}d}. \tag{3.58}$$

As before, application of the boundary condition (3.6) for $\phi = \phi_0 + \phi_1 + \phi_2$, expanding about $r = R_1$, while keeping the terms to the third order, leads to the following expression for ϕ_2:

$$\phi_2 = -\frac{\epsilon_1 4g}{\omega_{nm}}\sin\omega t\sum_{l=1}^{\infty}\frac{(-1)^l\eta\cos\alpha_l x\hat{\chi}_{0l}(\alpha_l r)}{(\alpha_l^2-\eta^2)\alpha_l d\hat{\chi}'_{0l}(\alpha_l R_1)} - \frac{4\epsilon_1 g}{\pi\omega_{nm}}\sin\omega t$$

$$-\epsilon_1\dot{\zeta}^{c,s}_{nm}(d_1 + \frac{g\cos\omega t}{\omega_{nm}^2})\sum_{l=1}^{\infty}G_{nl}\cos\alpha_l x\hat{\chi}_{nl}(\alpha_l r)\cos(n\theta) + O(\epsilon_1^2) \tag{3.59}$$

where $\epsilon_1 d_1 = a_0$, see (2.1). The constant coefficients G_{nl} are given by

$$G_{nl} = \frac{2k_{nm}^2}{\hat{\chi}'_{nl}(\alpha_l R_1)d\alpha_l N_{nm}\cosh k_{nm}d}\left[\chi''_{nm}(k_{nm}R_1)\int_{-d}^{0}\cosh k_{nm}(x+d)\cos\eta x\cos\alpha_l x\mathrm{d}x\right.$$

$$\left.+(\eta\chi_{nm}(k_{nm}R_1)/k_{nm})\int_{-d}^{0}\sinh k_{nm}(x+d)\sin\eta x\cos\alpha_l x\mathrm{d}x\right]. \tag{3.60}$$

The third term in (3.59) is $O(\epsilon_1^{3/2})$. It is found from the linear approximation of the nonlinear condition (3.3) that the amplitude of ϕ_1 is $\phi_{nm}(t) = \dot{\zeta}_{nm}(t)[k_{nm}\tanh(k_{nm}d)]^{-1} + O(\epsilon_1)$ (see (3.26)).

In order to let (3.42), (3.58) and (3.59) satisfy the kinematic boundary condition (3.3), this condition is Taylor-expanded, while retaining the terms up to the third order, namely to $O(\epsilon_1^{3/2})$, yielding

$$(\phi_0)_x + (\phi_1)_x + \zeta(\phi_0)_{xx} + \zeta(\phi_1)_{xx} + \zeta^2(\phi_1)_{xxx} + \zeta(\phi_2)_{xx} = \zeta_t + (\phi_1)_r\zeta_r + \frac{1}{r^2}(\phi_1)_\theta\zeta_\theta$$

$$+ (\phi_0)_r\zeta_r + (\phi_2)_r\zeta_r + \frac{1}{r^2}(\phi_2)_\theta\zeta_\theta + (\phi_1)_{rx}\zeta\zeta_r + \frac{1}{r^2}(\phi_1)_{\theta x}\zeta\zeta_\theta. \tag{3.61}$$

Substitution of (3.42), (3.58) and (3.59) then yields, after multiplying by $\psi_{nm}(r,\theta)/N_{nm}$ and integrating over the surface $x = 0$,

$$\phi_{nm}(t) = \gamma_{10}[1 - \gamma_{11}\zeta_{nm}^2]\dot{\zeta}_{nm} - \epsilon_1\gamma_{10}D\zeta_{nm}\sin\omega t + O(\epsilon_1^2), \tag{3.62}$$

with

$$\left.\begin{aligned}
&\gamma_{10} = [k_{nm}\tanh(k_{nm}d)]^{-1}; \quad \gamma_{11} = \frac{1}{N_{nm}^4}\int\int[k_{nm}^2\psi^2 - \psi_r^2 - \frac{1}{r^2}\psi_\theta^2]\psi^2 r\mathrm{d}r\mathrm{d}\theta;\\
&D = -D_{n0} + \sum_{l=1}^{\infty} D_{nl}; \quad D_{n0} = \frac{2gR_1k_{nm}}{\omega_{nm}(R_2^2 - R_1^2)N_{nm}^2}\int_{R_1}^{R_2}(r - \frac{R_2^2}{r})\chi'_{nm}\chi_{nm}r\mathrm{d}r;\\
&D_{nl} = \frac{4g\pi^2(-1)^l\eta}{(\alpha_l^2 - \eta^2)\omega_{nl}\hat{\chi}'_{nl}(\alpha_lR_1)dN_{nm}^2}\left[k_{nm}\int_{R_1}^{R_2}\hat{\chi}'_{nl}\chi'_{nm}\chi_{nm}r\mathrm{d}r + \alpha_j\int_{R_1}^{R_2}\hat{\chi}_{nj}\chi_{nm}^2 r\mathrm{d}r\right].
\end{aligned}\right\} \tag{3.63}$$

The term $\epsilon_1\gamma_{10}D\zeta_{nm}\sin\omega t$ expresses the influence of the potentials ϕ_0 and ϕ_2. This term can be classified as the one which gives rise to the parametric resonance in this mathematical problem. It is similar to an additional term $-(\epsilon_1\omega^2\cos\omega t)\zeta$ in the dynamical boundary condition (3.2) that arises for the case of parametric resonance in a tank that is subjected to a harmonic displacement ($\epsilon_1\cos\omega t$) along the vertical axis (note that this is equivalent to a harmonic modulation of the gravitational acceleration).

Equations (3.42), (3.55), (3.58), (3.59) and (3.62) are now substituted into the Taylor expansion of the expression for the dynamic boundary condition (3.2):

$$(\phi_0)_t + (\phi_1)_t + \zeta(\phi_1)_{tx} + (\phi_2)_t + \zeta^2(\phi_1)_{txx} + \zeta(\phi_0)_{tx} + \left(g + \frac{T}{\rho}\nabla^2\right)\zeta + (\phi_0)_r(\phi_1)_r$$

$$+\frac{1}{2}\left[(\phi_1)_x^2 + (\phi_1)_r^2 + \frac{1}{r^2}(\phi_1)_\theta^2\right] + (\phi_1)_x\zeta(\phi_1)_{xx} + (\phi_1)_r\zeta(\phi_1)_{rx} + \frac{1}{r^2}(\phi_1)_\theta\zeta(\phi_1)_{\theta x} + (\phi_1)_r(\phi_2)_r$$

$$+\frac{1}{2}\frac{T}{\rho}k_{nm}^2\zeta(\zeta_r^2 + \frac{1}{r^2}\zeta_\theta^2) + \frac{T}{\rho}\left\{\zeta_r\left[\zeta_r\zeta_{rr} - \frac{1}{r^3}\zeta_\theta^2 + \frac{1}{r^2}\zeta_\theta\zeta_{r\theta}\right] + \frac{1}{r^2}\zeta_\theta\left[\zeta_r\zeta_{r\theta} + \frac{1}{r^2}\zeta_\theta\zeta_{\theta\theta}\right]\right\} = F(t). \tag{3.64}$$

(Here we have some additional terms, which can also be classified as giving rise to the parametric resonance.) By averaging this expression over the fast time $\omega t/2$, after multiplication by $\psi(r,\theta)/N_{nm}$ and by integration over the surface $x = 0$, one derives

the following evolution equations:

$$\frac{dp_1}{d\tau_1} = -\hat{\alpha}p_1 - [\beta_1 - \beta_2 + \tfrac{1}{2}A_1(p_1^2 + q_1^2)]q_1 + \beta_3 q_1, \tag{3.65a}$$

$$\frac{dq_1}{d\tau_1} = -\hat{\alpha}q_1 + [\beta_1 - \beta_2 + \tfrac{1}{2}A_1(p_1^2 + q_1^2)]p_1 + \beta_3 p_1. \tag{3.65b}$$

Here

$$\beta_1 = \frac{2(\omega^2 - 4\omega_{nm}^2)}{\epsilon_1 \omega^2} \tag{3.66}$$

is a dimensionless parameter of the frequency differences. Furthermore,

$$\left.\begin{aligned}
&A_1 = \lambda_1^2(3\gamma_{12} - \gamma_{11} - \gamma_{13} - \gamma_{14});\\
&\gamma_{12} = \frac{k_{nm}^2}{N_{nm}^4}\int_0^{2\pi}\int_{R_1}^{R_2} \psi^4 r\,dr\,d\theta; \quad \gamma_{13} = \frac{1}{N_{nm}^4}\int_0^{2\pi}\int_{R_1}^{R_2}\left[k_{nm}^2(\psi^2) + \psi_r^2 + \frac{1}{r^2}\psi_\theta^2\right]\psi^2 r\,dr\,d\theta;\\
&\gamma_{14} = \frac{Tk_{nm}^3 \tanh k_{nm}d}{2\rho\omega^2 N_{nm}^4}\int_0^{2\pi}\int_{R_1}^{R_2}\left[\psi_r^2 + \frac{1}{r^2}\psi_\theta^2\right]\psi^2 r\,dr\,d\theta \int\left[\psi_r^2 + \frac{1}{r^2}\psi_\theta^2\right]\psi^2 r\,dr\,d\theta\\
&\quad + \frac{Tk_{nm}\tanh k_{nm}d}{\rho\omega^2 N_{nm}^4}\int_0^{2\pi}\int_{R_1}^{R_2}\left\{\psi_r\left[\psi_r\psi_{rr} - \frac{1}{r^3}\psi_\theta^2\right.\right.\\
&\quad \left.\left. + \frac{1}{r^2}\psi_\theta\psi_{r\theta}\right] + \frac{1}{r^2}\psi_\theta\left[\psi_r\psi_{r\theta} + \frac{1}{r^2}\psi_\theta\psi_{\theta\theta}\right]\right\}\psi r\,dr\,d\theta;
\end{aligned}\right\} \tag{3.67}$$

$$\beta_2 = \frac{2a_0}{a_1}\sum_{l=1}^{\infty} H_{nl}; \qquad \beta_3 = \frac{2}{\omega}\sum_{l=1}^{\infty} D_{nl} + \sum_{l=1}^{\infty} H_{nl} - \frac{2}{\omega}\sum_{l=1}^{\infty} F_{nl}; \tag{3.68}$$

$$H_{nl} = \frac{gG_{nl}\pi b_{nlm}}{\gamma_{10}\omega_{nm}^2}; \qquad F_{nl} = \frac{(-1)^l 8g\eta\pi^2 k_{nm}}{(\alpha_l^2 - \eta^2)\omega d N_{nm}^2 \hat{\chi}_{0l}'(\alpha_l R_1)}\int_{R_1}^{R_2} \hat{\chi}_{0l}'\chi_{nm}'\chi_{nm} r\,dr. \tag{3.69}$$

β_2 and β_3 are parameters that determine the fraction of energy transmitted by the vibrating shell into the cross-waves directly. Both parameters have terms that contain an integral over the surface of wavemaker, characterized by $a_1 \cos \eta x$, indicating that the wavemaker vibrations $a_1 \cos \eta x \cos \omega t$ cause the parametric resonance. Neither β_2 nor β_3 depends on the components of the potential ϕ_0 (3.42) in this approach. Both of them depend on the value of the pressure created by $(\phi_2)_t$, and β_3 is affected by the component of the fluid velocity $\zeta(\phi_2)_{xx}$ on the fluid free surface. We have already incorporated in (3.65) linear damping, as it was done in (3.51), and $\hat{\alpha} = \delta_{nm}/\epsilon_1$, with δ_{nm} the ratio of actual to critical damping of the dominant mode.

Evolutionary equations of the form (3.65) are characteristic of dynamic systems with parametric resonances (see Miles 1984*a*; Henderson & Miles 1990). The presence of the terms $\beta_3 p_1$ and $\beta_3 q_1$ indicates that we have parametric resonance and non-zero amplitudes of the dominant modes. The system (3.65) has a typical solution corresponding to harmonic vibrations (i.e. $dp_1/d\tau_1 = 0$ and $dq_1/d\tau_1 = 0$) for which

$$p_1^2 + q_1^2 = \frac{2}{A_1}[(\beta_2 - \beta_1) \pm (\beta_3^2 - \hat{\alpha}^2)^{1/2}]. \tag{3.70}$$

The stability of the fixed-point solution can be investigated by determining the roots of the characteristic equation, as was done by Miles (1984*a*).

At the beginning of this section we have made two assumptions: the first one about the close values of the frequencies ω and $2\omega_{nm}$, the second about approximating the free-surface patterns by the non-symmetric resonant eigenmode (3.54). Using these two assumptions, we obtained the expression (3.70) for the amplitude of the resonant mode. If the difference between ω and $2\omega_{nm}$ is not small (as for every non-resonant eigenmode), then β_1 is larger than any of the other coefficients in (3.65) (β_1 will be $O(\epsilon_1^{-2/3})$). In that case a fixed-point solution corresponds to zero values of the amplitudes p_1 and q_1. An extended analysis† of the non-axisymmetric resonant case, including secondary modes, has shown that the mean level oscillations and secondary modes may change the amplitude of the parametric excitation β_3 and the coefficient A_1 of the nonlinearity of the system (3.65). However, the change in the values may be negligibly small for the same 'geometrical' reason as for the value of ζ_{00}.

4. Comparison of theoretical results with laboratory observations

In the previous section the free-surface displacement $\zeta(r, \theta, t)$ has been analysed for the cases of the axisymmetric resonance mode, represented by (3.36), and the non-axisymmetric mode, as expressed by (3.54). We will now examine how the theoretical patterns compare with the observed resonance patterns as discussed in §2.

The first case that will be considered is axisymmetric resonance at the excitation frequency $f_e = 14.86$ Hz. In the laboratory experiment (see figure 5*a*) we observed a concentric pattern with 13 nodal circles. The axisymmetric $m = 13$ surface-elevation pattern according to (3.36) has been plotted in figure 5(*b*), with the dark bands representing areas with $\zeta > 0$, i.e. surface elevations. (Note that in figure 5*a* the surface elevations show up as white bands). The FFT of the wave gauge signal showed that the resonance occurs at the excitation frequency f_e – as expected – and this value should be compared with the eigenfrequency $f_{0m} = \omega_{0m}/2\pi$. For a proper comparison one should also take into account the effects of surface tension and the Stokes boundary-layer damping. According to Henderson & Miles (1990, 1991)

$$f_{nm} = (1 - \delta_{nm})\tilde{f}_{nm} = (1 - \delta_{nm})\frac{1}{2\pi}[k_{nm}(g + Tk_{nm}^2/\rho)\tanh k_{nm}d]^{1/2}, \tag{4.1}$$

where f_{nm} is the viscous-shifted frequency; δ_{nm} is the ratio of actual to critical damping; $\tilde{f}_{nm}$ is the inviscid frequency; $k_{nm} = k_{ij}$ is the eigen-number of the natural eigenfrequency, appearing as the root of (3.24); $i = n$ and $j = m$ are the wavenumbers in the circumferential and radial directions, respectively. Analytical expressions for δ_{nm} had the same components as used by Henderson & Miles (1990) for bottom and free-surface boundary layers. For a sidewall damping component we took analytical formulae derived by Miles (1967) and calculated the damping in the sidewall boundary layers for the annular tank at both the inner and outer cylinders. In the calculations we used $\nu = 0.03$ cm^{2}s^{-1} (this effective value of the kinematic viscosity was found by Henderson & Miles (1990) to yield the best agreement with the observed damping effects) and took into account the influence of a_0, so that the radius of the inner shell was $R_1 = r_1 + 2a_0/\pi$. The surface tension in (4.1) is represented by T, which for an air–fluid surface at 20°C for the dilute KCl solution used in the present experiments has a value of 68.9 dyn cm^{-1}, measured by a tensiometer K10ST.

For the case of direct excitation at a frequency $f_e = 14.86$ Hz one observes $i = n = 0$, $j = m = 13$. The experimentally observed wave pattern as well as the elevation

† This material can be obtained either directly from the authors or through the Editorial Office.

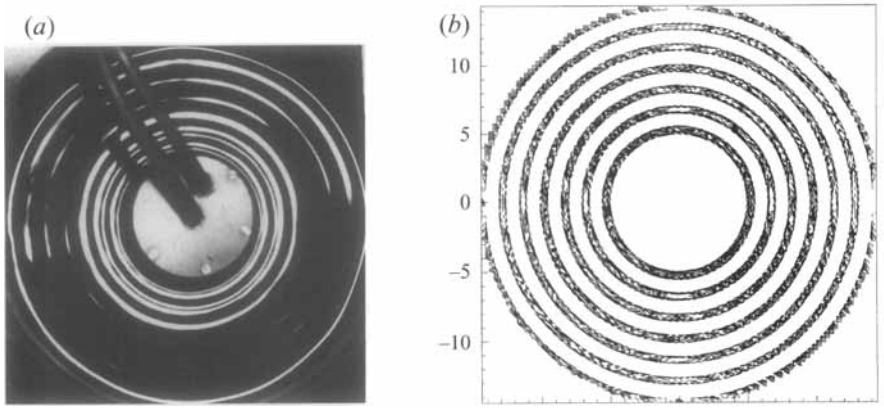

FIGURE 5. Axisymmetric wave pattern (*a*) observed in the laboratory for $f_e = 14.86$ Hz and (*b*) according to (3.36) for $i = n = 0$, $j = m = 13$.

	Observed mode		Theoretical values	
f_e (Hz)	n	m	Eigenfrequency (Hz)	Neighbouring eigenfrequencies (Hz)
(*a*)				
11.13	0	9	f_{09}=10.69	f_{08}=9.67; f_{010}=11.77
13.07	0	11	f_{011}=12.89	f_{010}=11.77; f_{012}=14.06
14.86	0	13	f_{013}=15.28	f_{012}=14.06; f_{014}=16.55
(*b*)				
21.82	17	8	f_{178}=11.17	f_{177}=10.57; f_{179}=11.88
26.00	20	10	f_{2010}=13.51	f_{209}=12.87; f_{2011}=14.46
27.01	22	9	f_{229}=13.62	f_{228}=12.86; f_{2210}=14.30
30.10	25	11	f_{2511}=16.21	f_{2510}=15.47; f_{2512}=16.99

TABLE 1. Eigenfrequencies of observed resonance modes: (*a*) forced resonance, (*b*) parametric resonance.

pattern according to (3.36) for $n = 0$, $m = 13$ are shown in figure 5. The expression (4.1) predicts $f_{013} = 15.28$ Hz, while the closest neighbouring eigenfrequencies are $f_{012} = 14.06$ Hz and $f_{014} = 16.55$ Hz (values are listed in table 1*a*). Obviously, the value of f_{013} lies closest to that of the excitation frequency $f_e = 14.86$ Hz, the difference being only 2.8% of f_e. The system apparently picks out the resonance frequency closest to the frequency of excitation.

A similar behaviour was observed for the case $f_e = 11.13$ Hz, in which 9 nodal circles arise (see figure 2*a*). According to (4.1), the eigenfrequency of this mode is $f_{09} = 10.69$ Hz, which is again close to the excitation frequency f_e (4% deviation).

Next, we will compare the non-symmetrical resonance patterns as observed in the laboratory with those predicted by (3.54). For the case $f_e = 26.00$ Hz (see figure 4) we measured $n = 20$ and $m = 10$. The experimentally observed wave pattern and the elevation pattern according to (3.54) for these n, m-values are shown in figure 6(*a*,*b*). Equation (4.1) predicts for this particular parametric resonance mode an eigenfrequency $f_{2010} = 13.51$ Hz, which is close to the value $0.5f_e = 13.0$ Hz (4% deviation). The closest neighbouring eigenfrequencies are $f_{209} = 12.87$ Hz and $f_{2011} = 14.46$ Hz, differing by 1% and 11%, respectively, from $0.5f_e$.

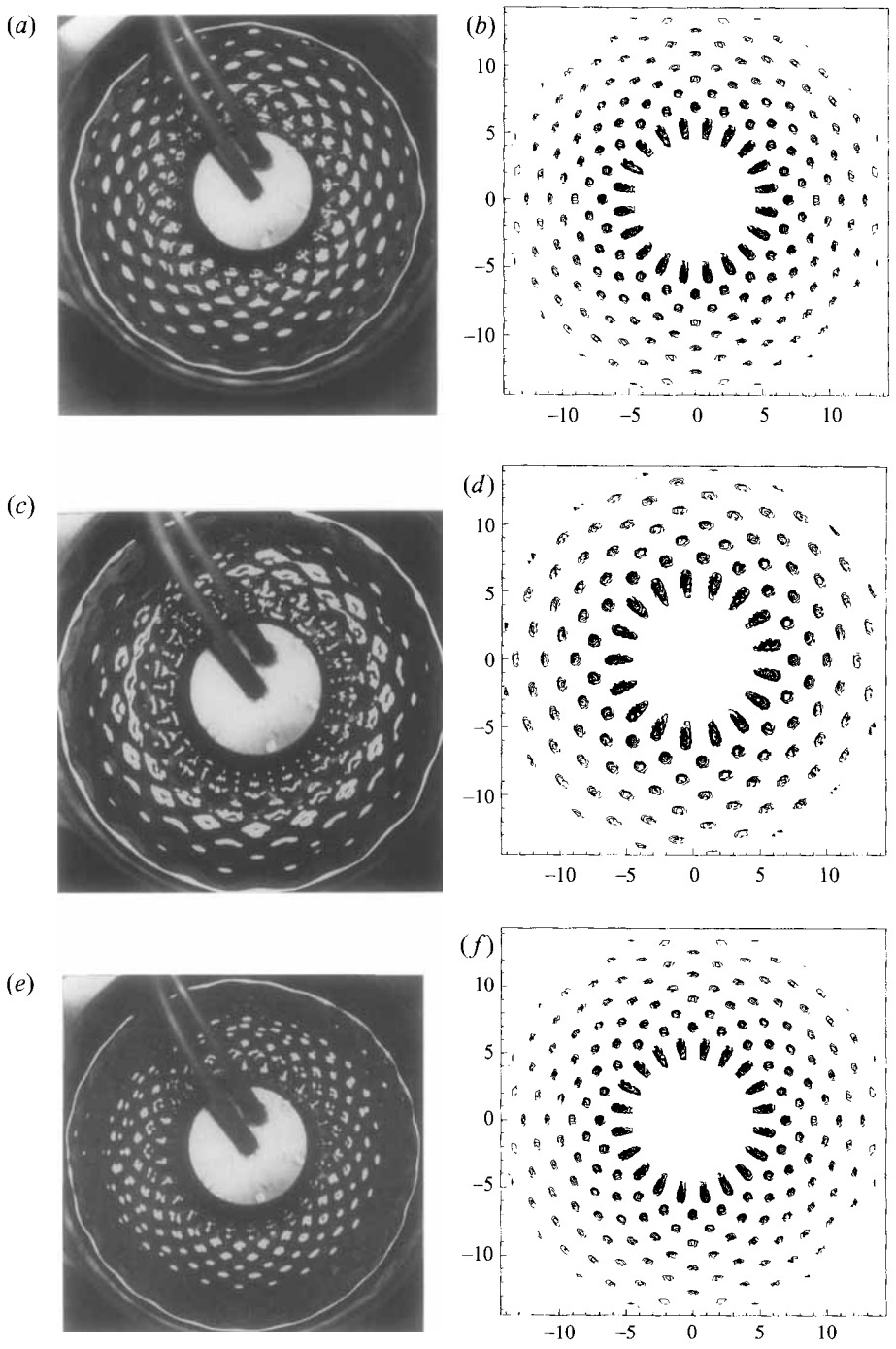

FIGURE 6. Comparison of parametrically excited resonance modes as observed in the laboratory with patterns predicted by (3.54). Laboratory observations for $f_e = 26.00$ Hz (*a*), 21.82 Hz (*c*), 31.10 Hz (*e*) and surface elevation patterns according to (3.54) for (*b*) $l = 20$, $m = 10$; (*d*) $n = 17$, $m = 8$; (*f*) $n = 25$, $m = 11$.

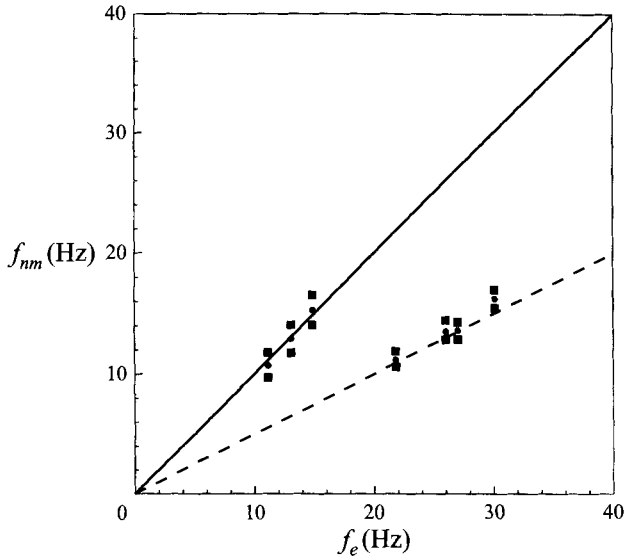

FIGURE 7. Frequencies of the observed resonant wave patterns for different f_e-values. The frequencies have been calculated using (4.1) for the observed mode (n, m), as indicated by the bullets; the filled squares represent closest neighbouring frequencies. The solid and the broken lines represent $f = f_e$ and $f = 0.5f_e$, respectively.

A similar comparison for the case f_e=21.82 Hz is presented in figures 6(*c*) and 6(*d*). The frequency corresponding to this mode is $f_{178} = 11.17$ Hz, which lies close to $0.5f_e$ (within 2%) and which characterizes the minimum value of the function $\delta_{17m} = \delta_{178}$ necessary for the realization of the mode ξ_{178} in the experiment (see, Henderson & Miles 1990, 1991). Values of the closest neighbouring eigenfrequencies are given in table 1(*b*).

The observed and theoretical resonance pattern for $f_e = 30.10$ Hz are shown in figures 6(*e*) and 6(*f*). Again, the correspondence between the patterns as well as between the frequencies (see table 1*b*) is good. Although the frequencies of the observed resonant wave patterns (as well as their closest neighbouring values) are listed in table 1(*b*), for convenience they are also presented graphically in figure 7 as a function of the excitation frequency f_e. The bullets represent the frequencies calculated from (4.1) for the observed n,m-mode, whereas the closest neighbouring frequencies are denoted by filled squares. The graph nicely demonstrates the good correspondence with the frequencies f_e (solid line) and $0.5f_e$ (broken line) for the axisymmetric, forced resonance and the non-axisymmetric, parametric resonance, respectively. Note that for higher excitation frequencies the theoretical values are slightly larger than the measured ones. This small discrepancy is attributed to the approximative character of the modelling of the damping effects in (4.1).

The laboratory experiments were carried out at the Fluid Dynamics Laboratory in Eindhoven. The authors gratefully acknowledge Eep van Voorthuisen and Jan Willems for the designing and building of the experimental set-up. We thank Dr Adel Elyousfi for helpful comments and surface tension measurements. We are indebted to Professor Vyacheslav Meleshko for general discussions and suggestions connected with the Lamé method. Also, the useful comments of the referees are thankfully acknowledged.

Appendix. The integrals and coefficients of the equations for symmetrical patterns

The coefficients of equations (3.32), (3.34) and (3.35) are related with integration over the radial distance between the cylinders in the following manner:

$$\gamma_1 = \frac{2\gamma_0\pi}{N_{0m}^3}\int_{R_1}^{R_2}\psi_1\psi_{0m}r\mathrm{d}r, \qquad \gamma_2 = \gamma_0\left(\gamma_1^2 - \frac{2\pi}{N_{0m}^4}\right)\int_{R_1}^{R_2}\psi_1\psi_{0m}^2 r\mathrm{d}r,$$

$$\psi_1 = k_{0m}^2\psi_{0m}^2 - [(\psi_{0m})_r]^2,$$

$$\gamma_3 = 2\gamma_1 - \gamma_5\gamma_0 - \gamma_6, \qquad \gamma_4 = \gamma_6 - \gamma_5\gamma_0,$$

$$\gamma_5 = \frac{1}{2\gamma_0}\gamma_6 + \frac{\pi}{N_{0m}^3}\int_{R_1}^{R_2}[(\psi_{0m})_r]^2\psi_{0m}r\mathrm{d}r, \qquad \gamma_6 = \frac{2\pi}{N_{0m}^3\gamma_0}\int_{R_1}^{R_2}\psi_{0m}^3 r\mathrm{d}r,$$

$$\gamma_7 = \frac{2\pi k_{0m}^2}{N_{0m}^4}\int_{R_1}^{R_2}\psi_{0m}^4 r\mathrm{d}r, \qquad \gamma_8 = \gamma_7 + \frac{2\pi}{N_{0m}^4}\int_{R_1}^{R_2}[(\psi_{0m})_r]^2\psi_{0m}^2 r\mathrm{d}r,$$

$$A = \frac{\lambda^2}{2}\left(\frac{\gamma_2}{\gamma_0} - 2\gamma_7\gamma_1 + 2\gamma_8\gamma_1 + 3\gamma_5 - \gamma_6\right) + \frac{\lambda}{6}[(\gamma_3 + 2\gamma_4)^2 + 3\gamma_3\gamma_4].$$

REFERENCES

BECKER, J. M. & MILES, J. W. 1991 Standing radial cross-waves. *J. Fluid Mech.* **222**, 471–499.

BECKER, J. M. & MILES, J. W. 1992 Progressive radial cross-waves. *J. Fluid Mech.* **245**, 29–46.

BROMWICH, T. J. I. 1959 *An Introduction to the Theory of Infinite Series.* London: Macmillan.

FARADAY, M. 1831 On a peculiar class of acoustical figures; and on certain forms assumed by groups of particles upon vibrating elastic surfaces. *Phil. Trans. R. Soc. Lond.* A **121**, 299–340.

FRYER, D. K. & THOMAS, M. W. S. 1975 A linear twin wire probe for measuring water waves. *J. Phys.* E: *Sci. Instrum.* **8**, 405–408.

GARRETT, C. J. R. 1970 Cross waves. *J. Fluid Mech.* **41**, 837–849.

HAVELOCK, T. H. 1929 Forced surface waves on water. *Phil. Mag.* (7) **8**, 569–576.

HENDERSON, D. M. & MILES, J. W. 1990 Single-mode Faraday waves in small cylinders. *J. Fluid Mech.* **213**, 95–109.

HENDERSON, D. M. & MILES, J. W. 1991 Faraday waves in 2:1 resonance. *J. Fluid Mech.* **222**, 449–470.

HOCKING, L. M. 1988 Capillary-gravity waves produced by a heaving body. *J. Fluid Mech.* **186**, 337–349.

HOCKING, L. M. & MAHDMINA, D. 1991 Capillary-gravity waves produced by a wavemaker. *J. Fluid Mech.* **224**, 217–226.

KRASNOPOLSKAYA, T. S. & PODCHASOV, N. P. 1992*a* Waves in a liquid between two coaxial cylindrical shells induced by vibrations of the inner cylinder. *Intl Appl. Mech.* **28**, 188–195.

KRASNOPOLSKAYA, T. S. & PODCHASOV, N. P. 1992*b* Forced oscillations of a liquid between two cylinders excited by vibrations of an inner shell. *Intl Appl. Mech.* **28**, 240–245.

LAMB, H. 1932 *Hydrodynamics.* Cambridge University Press.

LAMÉ, G. 1852 *Leçons sur la Théorie Mathématique de l'Élasticité des Corps Solids.* Bachelier, Paris.

LEBEDEV, N. N., SKAL'SKAYA, I. P. & UFLYAND, YA. S. 1966 *Problems in Mathematical Physics.* Oxford: Pergamon.

LUKE, J. C. 1967 A variational principle for a fluid with a free surface. *J. Fluid Mech.* **27**, 395–397.

MILES, J. W. 1967 Surface-wave damping in closed basins. *Proc. R. Soc. Lond.* A **297**, 459–475.

MILES, J. W. 1984*a* Nonlinear Faraday resonance. *J. Fluid Mech.* **146**, 285–302.

MILES, J. W. 1984*b* Internally resonant surface waves in a circular cylinder. *J. Fluid Mech.* **149**, 1–14.

MILES, J. W. 1984*c* Resonantly forced surface waves in a circular cylinder. *J. Fluid Mech.* **149**, 15–31.

MILES, J. W. & HENDERSON, D. 1990 Parametrically forced surface waves. *Ann. Rev. Fluid Mech.* **22**, 143–165.

TANEDA, S. 1991 Visual observation of the flow around a half-submerged oscillating sphere. *J. Fluid Mech.* **227**, 193–209.

TANEDA, S. 1994 Visual observations of the flow around a half-submerged oscillating circular cylinder. *Fluid Dyn. Res.* **13**, 119–151.

TATSUNO, M., INOUE, S. & OKABE, J. 1969 Transfiguration of surface waves. *Rep. Res. Inst. Appl. Mech.* **17**, 195–215.